Morphology Evolution of TiO$_2$ Facets and Vital Influences on Photocatalytic Activity

Lun Pan, Ji-Jun Zou,* Songbo Wang, Xin-Yu Liu, Xiangwen Zhang, and Li Wang

Key Laboratory for Green Chemical Technology of the Ministry of Education, School of Chemical Engineering and Technology, Tianjin University, Tianjin 300072, China

S Supporting Information

ABSTRACT: Modulation of anatase toward highly active facets has been attracting much attention, but the mechanism and photoactivity are still ambiguous. Here we demonstrate the inherent mechanisms for facets nucleation and morphology evolution, and clarify some vital influences of facets and surface nature on the photoactivity. Simply tuning the Ti/F ratio in the synthetic mixture leads to single anatase crystal exposed with different facets like {001}, {010}, or {110}. And complex sphere structure exposed with {001} facets can be formed by secondary nucleation and growth. Prolonging the hydrothermal treatment time causes selective etching on {001} facets, whereas defluorination via thermal calcination produces many pores on the surface. The photodegradation of positively and negatively charged, and zwitterionic dyes indicates that the type of reactant, adsorption mode and surface area play significant roles in photocatalysis. This work makes a step toward understanding the formation of facet-mediated structure and designing highly active materials for environmental remediation, hydrogen production, and dye-sensitized solar cells.

KEYWORDS: photocatalysis, crystal growth, titanium dioxide, facets, morphology
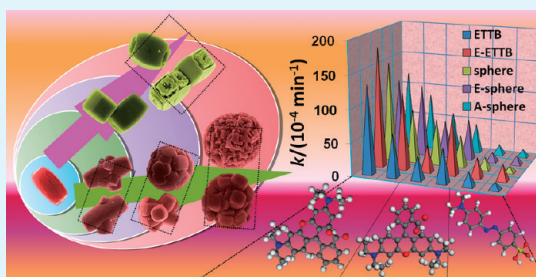
1. INTRODUCTION

Modulation of polyhedral morphology toward highly active facets has been considered as an important strategy to significantly promote the catalytic activity of noble metals, metal oxides, and semiconductors.[1−9] However, the crystal growth process based on minimization of surface energy leads to the disappearance of highly active facets,[1−5] especially for TiO$_2$ anatase.[10−13] Under the equilibrium condition, anatase crystal contains majority of {101} facets, along with minority of {001} facets.[10−14] Yang et al. made a breakthrough in synthesizing truncated tetragonal bipyramid (TTB) anatase with highly exposed {001} facets by fluorine capping.[10] Then, lots of works were dedicated to {001} anatase with various shapes, such as single particle, nanosheet, cube, film, and flowerlike sphere.[15−30] Recently, elongated truncated tetragonal bipyramid (ETTB) anatase with highly exposed {010} facets was also synthesized by tuning the Ti/F ratio.[14]

Contrary to the intense investigations on the preparation of specific facets, the inherent photoactivities of TiO$_2$ facets are still ambiguous. The {001} facet was initially expected to be most active because of its high surface energy,[10,15−32] whereas later work suggested that the clean {010} facet with 100% five-coordinate Ti was more active in photo-oxidation and photo-reduction reactions.[14] However, more recently works suggested that different facets may play different roles in photo-reaction.[33,34] In addition, adsorption mode of reactants on the semiconductor was reported to play an important role in photocatalytic reactions.[35−37]

The present work includes two parts. First, we will illuminate the nucleation and growth mechanisms from {010} single crystal to highly exposed {001} sphere, along with further evolution of local morphology by post-treatment. Second, we will discuss some important factors influencing the photo-activity of synthesized crystals via the photodegradation of positively charged, negatively charged and zwitterionic dyes. This work is expected to make a step toward understanding the formation of facet-mediated structure and designing highly active materials for environmental remediation, hydrogen production, and dye-sensitized solar cells.

2. EXPERIMENTAL SECTION

2.1. Materials. Rhodamine B (RhB, positively charged dye), methyl orange (MO, negatively charged dye), titanyl sulfate (TiOSO$_4$·2H$_2$O), hydrofluoric acid (HF, 40 wt %), and sodium hydroxide (NaOH) were all reagent grade and purchased from Tianjin Guangfu Fine Chemical Research Institute. Rhodamine B base (RhB base, 99%, zwitterionic dye) was purchased from Acros Organics. Deionized water was used in all experiments. All the reagents were used as received.

2.2. Sample Preparation. The preparation of sample was based on the work reported by Pan et al.[14] In a typical synthesis route, 80 mL of 4.56 × 10^{-2} M HF aqueous solution was mixed under vigorous stirring (Caution! Hydrofluoric acid is extremely corrosive and a contact poison, and it should be handled with extreme care). Into the

Scheme 1. Structural Formula of Rhodamine B (RhB), Methyl Orange (MO), and Rhodamine B Base (RhB base)

Rhodamine B (RhB)　　　Methyl Orange (MO)　　　Rhodamine B base (RhB base)
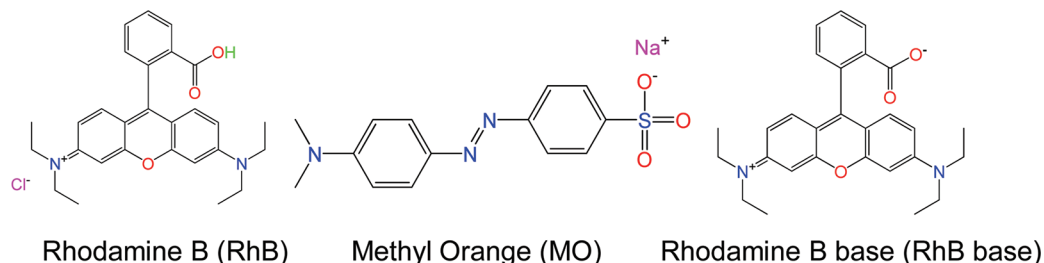
mixture, m_{Ti} (m_{Ti} = 32, 48, 64, and 128) mg of TiOSO$_4$ was added, and the suspension was stirred for 20 min. Then it was transferred to a 100 mL Teflon−lined autoclave and heated at 180 °C for t_h (t = 1, 2, 4, 6, 12, and 18) hours, respectively. After the hydrothermal process, the products were collected by centrifugation and washed with deionized water for several times. The samples were then dried overnight at 60 °C in air.

NaOH Washing Procedure. One-tenth of a gram of as-prepared sample was dispersed in 20 mL of 10 M NaOH aqueous solution under vigorous shaking for 30 min in an ultrasonic cleaner. The sample was then centrifuged and washed 5 times with deionized water.

Calcination Procedure. The samples were calcined at 600 °C for 2 h at a heating rate of 10 or 1 °C min^{-1}.

2.3. Characterizations. XRD characterizations were conducted using a D/MAX−2500 X−ray diffractometer equipped with Cu Kα radiation. Specific surface area (S_{BET}) was calculated based on N$_2$ adsorption/desorption isotherms using a Micromeritics TriStar 3000 at 77 K. All samples were outgassed under vacuum at 200 °C for 4 h. SEM images were observed using a field−emission scanning electron microscope (Hitachi S-4800), and spot energy dispersive spectrometry (EDS) were conducted to determine the surface atom content of F element. High-resolution TEM observations were carried out with a Tecnai G^2 F-20 transmission electron microscope. Selected-area electron diffraction (SAED) patterns were derived from JEM−100CX II electron microscope (JEOL).

2.4. Photocatalytic Reaction. Three dyes, including RhB, MO, and RhB base (Scheme 1), were used as mode reactants. Photo-degradation of dyes were conducted in a quartz chamber (150 mL) vertically irradiated by a 300 W high-pressure xenon lamp (PLS-SXE300UV, Beijing Trusttech. Co. Ltd.) located on the upper position. UV light (<450 nm) and visible light (>420 nm) were separated by UV−ref and UV−cut optical filters (Beijing Trusttech. Co. Ltd., Figure S1 in the Supporting Information), respectively. The intensity is 32.4 ± 0.5 mW cm^{-2} at the characteristic wavelength of 365 nm for UV light, and 13.0 ± 0.5 mW cm^{-2} at the characteristic wavelength of 420 nm for visible light, as determined by UV radiometer (photoelectric instrument factory of Beijing Normal University). The irradiation area of the light source was ca. 20 cm^2. Reaction conditions are as follows: temperature, 20 ± 2 °C; C_0(RhB)= C_0(RhB base)= 20 μmol L^{-1}, C_0(MO) = 120 μmol L^{-1}, TiO$_2$, 0.1 g L^{-1}. Photoreaction was conducted by magnetic stirring under open air conditions, after stirring for 20 min in the dark to achieve adsorption equilibrium. Samples were withdrawn at intervals and centrifuged immediately, then the supernatant was analyzed using Hitachi U−3010 UV−vis spectrometer.

3. RESULTS AND DISCUSSION

3.1. Facet Evolution. XRD characterization confirms that the prepared materials possess high purity of anatase phase (see Figure S2 in the Supporting Information). The percentage of crystallographic facet relies on the relative stability of each surface during crystal growth, intrinsically determined by the surface energy.[1−4] Experimental and theoretical work already confirms that the capping with F can lower the energy of {001} facets.[10] It is found that, in this work, simply tuning the Ti/F ratio produces dramatically different morphology with various

facets (Figure 1a−c). Low Ti/F ratio leads to unique and well crystallized TTB exposed with high percentage of {001} facets
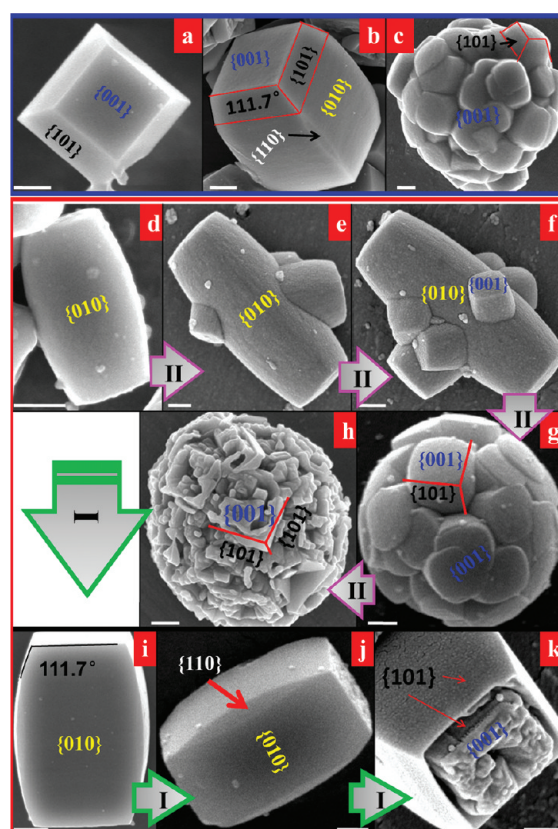

Figure 1. Evolution of anatase facets and morphology. Tunable shapes from (a) TTB to (b) ETTB and (c) {001} sphere with initial TiOSO$_4$ amount m_{Ti} controlled from 32 to 48 and 128 mg, respectively. Their hydrothermally treated time (t_h) are 18, 4, and 2 h, respectively; Crystal growth process of ETTB particles (pathway I) and {001} sphere (pathway II) with m_{Ti} = 64 mg and t_h of (d) 1, (e, f, i) 2, (g, j) 4, and (h, k) 12 h. All scale bars are 200 nm.

(Figure 1a). Increasing the ratio generates additional quartet column exposed with {010} facets between the two TTBs, namely ETTB (Figure 1b). Interestingly, further increasing the ratio forms sphere majorly exposed with {001} facets (Figure 1c). HR−TEM characterization shown in Figure 2 also supports the formation of the facets mentioned above. The fringes spacing of 4.8 Å on the top or bottom surface of the particle refers to the truncated {001} surface. The angle of 111.7° between the top square and the lateral trapezoid (Figure 1b,i) and the angle of 68.3° from SAED patterns (Figure 2) are both assigned to the angle between {101} and {001} facets.[14,32]
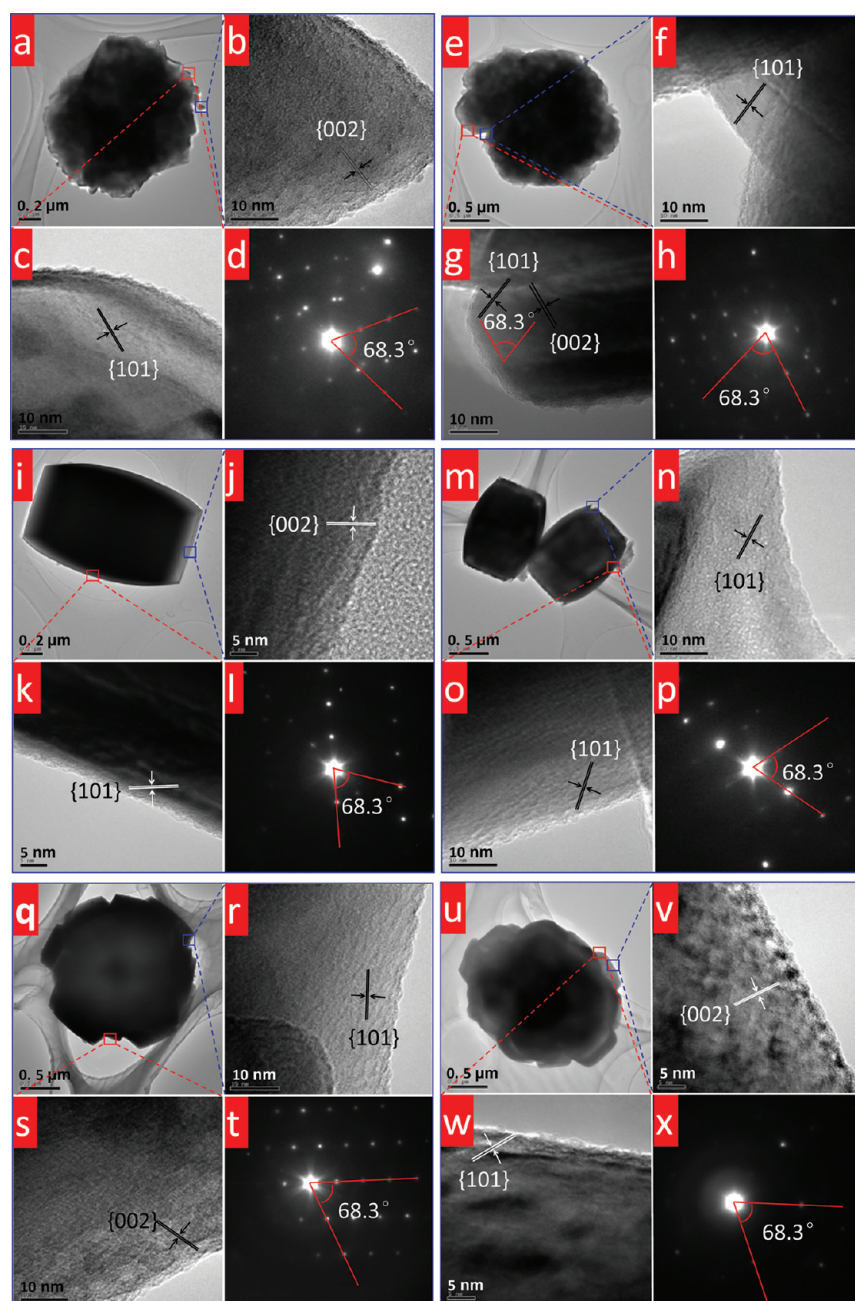
Figure 2. HR-TEM images and SAED patterns of anatase: (a–d) {001} sphere; (e–h) etched {001} sphere; (i–l) ETTB; (m–p) etched ETTB; (q–t) alkaline-treated {001} sphere; (u–x) calcined {001} sphere.

To understand the mechanisms of facet evolution, we synthesized serial samples using intermediate Ti/F ratio. Interestingly, a watershed is observed where ETTB and sphere are formed in two separate pathways, as illustrated in Figure 1d–k. Initially, ETTB seeds exposed with major {010} and minor {001} facets are quickly nucleated (Figure 1d), which is the starting point for the two evolution pathways. In pathway I (d → i → j → k), the seed grows into nice crystal with some {110} facets formed on the axial ribs; and further hydrothermal treatment causes selective erosion of {001} facets. In pathway II (d → e → f → g → h), some mini-TTB seeds exposed with {001} facets emerge on the "waist" of {010} column. These seeds burgeon quickly and fill up the space around the column, thus spheres highly exposed with {001} facets are formed.

Further prolonging the time also leads to the selective erosion of {001} facets.

The formation of sphere is a result of secondary nucleation and growth, in which F elements may also play the very important role. Selected-point EDS in Figure 3 shows an interesting distribution of F on the {010} surface of ETTB seed. There are more F on the two ends (1 and 8) of the column, and less on the "waist" (4, 5, and 6). It suggests that not only the Ti/F ratio in the synthetic solution but also the amount of surface-capping F is vital for the facet and morphology transformation. After the nucleation of ETTB seeds, further extending of {010} surface along the [001]-zone direction is inhibited by the terminated high−concentration F ions. And the Ti/F ratio in the remained aqueous solution becomes much lower than the initial ratio because many Ti ions
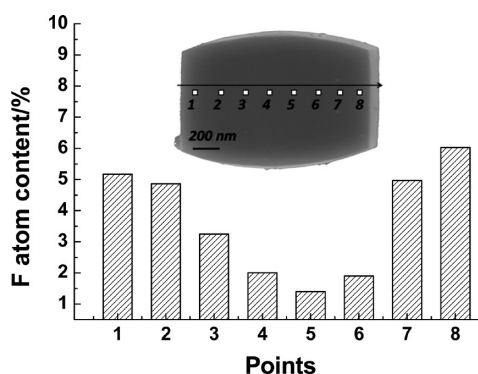
Figure 3. Atom content of fluorine on {010} facet of ETTB seed obtained by selected-point EDS.

have been consumed by surface capping. At this stage, the formation of TTB seeds becomes favorable again, like the case of Figure 1a. The "waist" of {010} column capped with less F is relatively clean and unstable, thus providing the active sites for the secondary nucleation and growth of TTB, finally with the {001} sphere crystallized.

3.2. Surface Morphology Evolution. The change of surface morphology of facets is another interesting phenomenon worthy of note. The first one is the selective erosion of {001} facet with prolonged hydrothermal treatment time (Figure 1h, k; Figure 2e−h, m−p). According to the DFT calculations by Wang et al.,[18] under low Ti/F ratio, HF can selectively destroy the {001} surface through the surface −OH replacement and −TiOF$_2$ dissolution processes. At the late stage of the present synthesis, the Ti/F ratio should be very low because most of the Ti ions are already built in the particles, so the chemical etching occurs. The dissolution−diffusing process was also reported by Yu et al.[38,39] They found that the fluoride causes both the dissolution of the interior TiO$_2$ and the subsequent mass transfer to the surface, and hollow TiO$_2$ sphere could be formed in the hydrothermal process.

More importantly, the post-defluorination treatment also has great influence on the surface morphology (Figure 2, Figure 4). Both alkaline washing and thermal calcination were used to remove the surface−capping F ions. The two methods can both effectively remove the surface-capping F, as determined by XPS and EDS (data not shown here), which was also verified by Liu et al.[15] Alkaline treatment does not change the surface morphology (Figure 4i,j). However, the thermal calcination generates many regular rectangle pores on the surface, especially on the {001} facets. The possibility of thermal expansion is excluded because different heating rates produce the same pores (see Figure S3 in the Supporting Information). The pore-forming should be attributed to the escape of F ions during the calcination process, although the mechanism is still not clear. And the amount of pores should depend on the amount of surface−capping F. Actually, the pores on the {001} facets are more obvious, due to the high content of surface F. For the etched samples, the calcination−induced pores are not obvious in the SEM images, compared with the existing erosion cracks (Figure 4c,d,g,h). A few pores are also present on the calcined alkaline−washed samples (Figure 4k,l), because of the removal of F ions remained in the interior. N$_2$−sorption data in Figure 5 support the formation of pores in the range of 50−200 nm. As a result, the surface area of calcined sample (4.31 m^2/g) is ca. 10 times larger than that of the etched counterpart (0.50
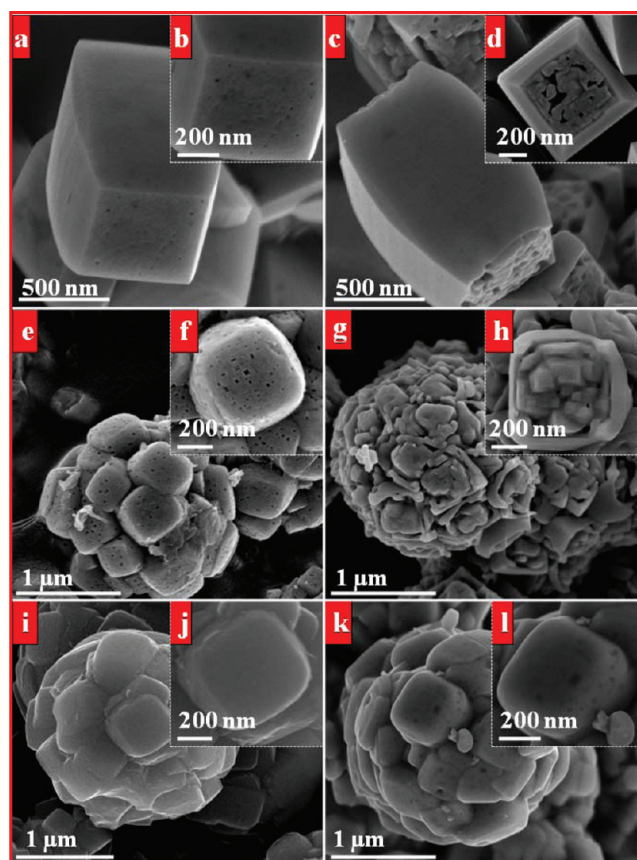

Figure 4. Surface morphology of TiO$_2$ anatase controlled by erosion, calcination, and alkaline treatment. (a, b) calcined ETTB, m_{Ti} = 48 mg, t_h = 4 h; (c, d) calcined etched ETTB, m_{Ti} = 48 mg, t_h = 12 h; (e, f) calcined {001} sphere, m_{Ti} = 128 mg, t_h = 2 h; (g, h) calcined etched {001} sphere, m_{Ti} = 128 mg, t_h = 12 h; (i, j) alkaline-washed {001} sphere, m_{Ti} = 128 mg, t_h = 2 h; (k, l) calcined alkaline-washed {001} sphere, m_{Ti} = 128 mg, t_h = 2 h.
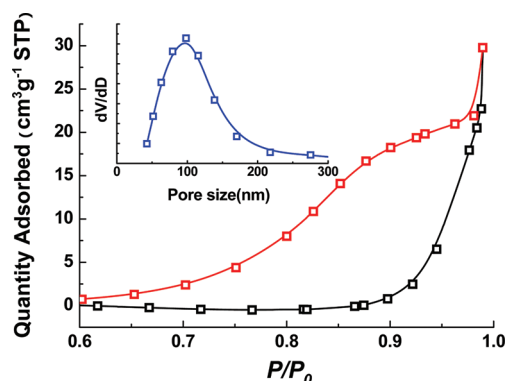

Figure 5. N$_2$ adsorption−desorption isotherms and pore distribution (inset) of the calcined {001} sphere.

m^2/g). This is very promising because high surface area is always favorable for photoreaction.

3.3. Influences on Photocatalytic Activity. To figure out the influences of surface facets and morphology on the photoactivity of anatase, we evaluated the photodegradation of charged (RhB and MO) and zwitterionic (RhB base) dyes over ETTB and sphere with various local morphologies under UV and visible light irradiation. Five typical samples were prepared for the photoreaction. Their preparation conditions

and abbreviations are shown in Table 1, and the SEM images of prepared samples as well as their calcined counterparts are

Table 1. Preparation Conditions and Abbreviations of Samples Applied for Photodegradation

samples	abbreviations	m_{Ti} (mg)	t_h (h)
elongated truncated tetragonal bipyramid	ETTB	48	4
etched ETTB	E−ETTB	48	12
{001} sphere	sphere	128	2
etched {001} sphere	E−sphere	128	12
alkaline-washed sphere	A−sphere	128	2

shown in Figure S4 (see the Supporting Information). The reaction kinetic constant (k) shown in Figure 6 was derived from pseudo-first-order fitting of the data in Figure S5 (see the Supporting Information) and used for evaluating the photo-activity of the samples. We also compared the activity of prepared sample with standard Degussa P-25 under identical conditions. The apparent activity of TiO$_2$ in this work is lower than P-25 because of the very low surface area. But its normalized reaction rate divided by the surface area is significantly higher than that of P-25 (see Figure S6 in the Supporting Information), which agrees with the reported result.[21]

Effect of Adsorption Mode. There are several modes for the organics on the host surfaces such as covalent attachment and electrostatic interactions (via ion exchange, ion-pairing, or donor−acceptor interactions).[40,41] In this work, the presence or absence of surface F can significantly change the adsorption mode and thus the photoactivity. The comparison between sphere and A−sphere shows that removing surface F by alkaline washing promotes the photoactivity of all samples in the photodegradation of anionic dye, but suppresses that of cationic dye. On pure and clean surface, reactant is generally adsorbed

via physical or covalent coupling.[35,36] The presence of surface F$^−$ ions enhances the adsorption of cationic reactant via the newly formed electrostatic−adsorption mode, but is unfavorable for the adsorption of anionic reactants. The promotion of photoactivity via electrostatic adsorption mode was also reported previously.[36,37] It is worthy noting that, RhB base is a zwitterionic organic compound with both negatively (COO$^−$) and positively charged (R = N$^+$(C$_2$H$_5$)$_2$) moieties, so it is expected to be anchored on TiO$_2$ surface with any of the moieties or both. But the result shows that the behavior of RhB base is very like that of MO, suggesting that its adsorption mode is via COO$^−$ groups.

Some works showed that surface-capping F ions on nanosized TiO$_2$ can reduce the recombination of photo-generated electrons and holes, enhance the formation of hydroxyl radicals and finally improve the photocatalytic oxidation of some organics, because of its strong electron-withdrawing ability.[42,43] In the present case, however, such effect is not obvious. The reason may be that the prepared samples have very low surface area and the surface related processes, like adsorption of dyes, are rate-determining.

Surface Area vs Adsorption Mode. Thermal calcination brings two changes on the F-capped samples: removal of surface F and increase of surface area. Obviously, it benefits the photodegradation of anionic reactants, and the photodegradation of zwitterionic RhB base is also improved. However, for cationic reactant, the changes of adsorption mode and surface area show the opposite effects. The photoactivities of ETTB and E−ETTB with low percentage of {001} facets are decreased because the effect of surface area increase is very limited. So the change of adsorption mode is determinative in this case. The photoactivity of E−sphere keeps almost unchanged before and after thermal calcination, indicating the increased surface area compensates the eliminated electrostatic adsorption. For sphere, the significant increase in surface area
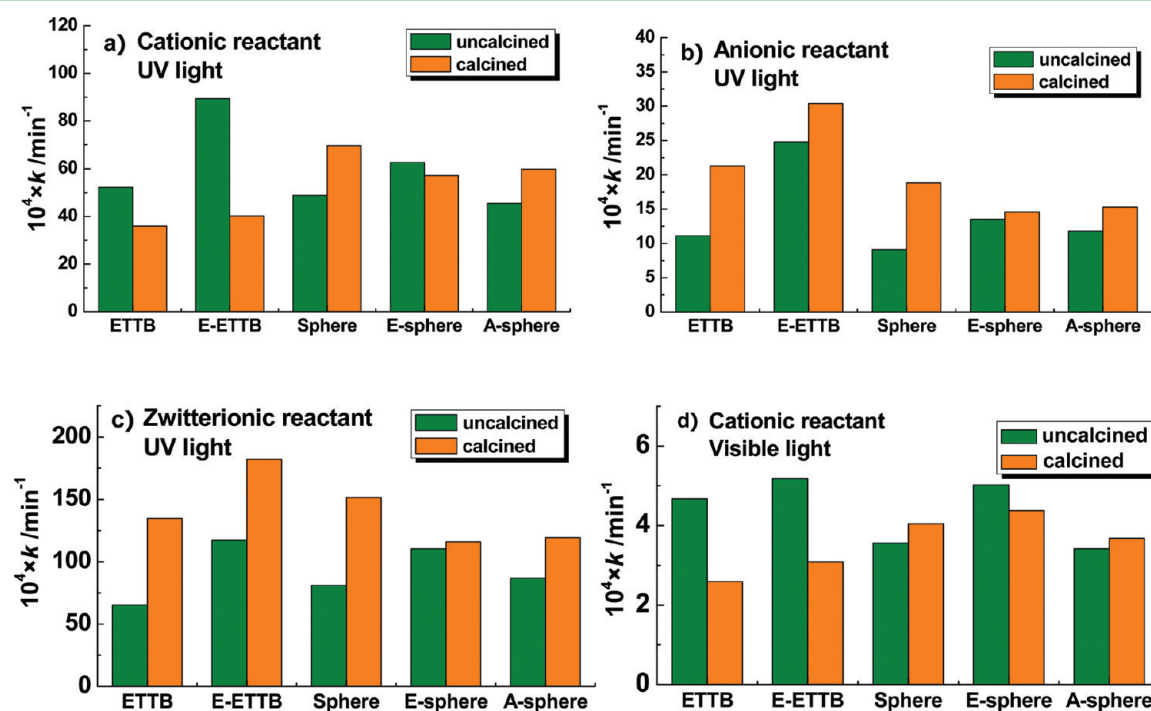

Figure 6. Photoactivity of anatase in degradation of (a) cationic RhB, (b) anionic MO, and (c) zwitterionic RhB base under UV light and (d) degradation of RhB under visible light.

due to the newly formed regular pores becomes the dominant factor, and the photoactivity is greatly enhanced. Additionally, solely increasing the surface area of A−sphere by thermal calcination leads to considerable improvement in photo-degradation of all dyes, verifying the positive function of calcination−induced pores.

4. CONCLUSIONS

During hydrothermal synthesis of TiO$_2$, the nucleation and growth of facets, formation of complex structure, and selective etching of {001} facets are dominated by the concentration of aqueous and surface-capping F. By simply tuning Ti/F ratio, we can fabricate single crystal exposed with {001}, {010}, or {110}, and sphere with {001} facets. Thermal calcination shows dual effects of defluorination and pore-generation, greatly increasing the surface area of resulting materials. The photoreactivity depends on the type of reactant, adsorption mode, and surface area. Tuning the facets composition and surface chemistry would be the keys to synthesize highly active anatase.

■ ASSOCIATED CONTENT

Ⓢ Supporting Information

The optical properties of UV−ref and UV−cut optical filters, XRD, SEM images, and photodegradation data of the as-prepared samples. This material is available free of charge via the Internet at http://pubs.acs.org.

■ AUTHOR INFORMATION

Corresponding Author
*E-mail: jj_zou@tju.edu.cn.

Notes
The authors declare no competing financial interest.

■ ACKNOWLEDGMENTS

■ REFERENCES

(1) Tian, N.; Zhou, Z.-Y.; Sun, S.-G.; Ding., Y; Wang, Z. L. *Science* **2007**, *316*, 732−735.
(2) Lim, B.; Jiang, M.; Camargo, P. H. C.; Cho, E. C.; Tao, J.; Lu, X.; Zhu, Y.; Xia, Y. *Science* **2009**, *324*, 1302−1305.
(3) Joo, J.; Chow, B. Y.; Prakash, M.; Boyden, E. S.; Jacobson, J. M. *Nat. Mater.* **2011**, *10*, 596−601.
(4) Xia, Y.; Xiong, Y.; Lim, B.; Skrabalak, S. E. *Angew. Chem., Int. Ed.* **2009**, *48*, 60−103.
(5) Jiang, H. B.; Cuan, Q.; Wen, C. Z.; Xing, J.; Wu, D.; Gong, X.-Q.; Li, C.; Yang, H. G. *Angew. Chem., Int. Ed.* **2011**, *50*, 3764−3768.
(6) Dong, J. J.; Zhang, X. W.; Yin, Z. G.; Zhang, S. G.; Wang, J. X.; Tan, H. R.; Gao, Y.; Si, F. T.; Gao, H. L. *ACS Appl. Mater. Interfaces* **2011**, *3*, 4388−4395.
(7) Kiatkittipong, K.; Scott, J.; Amal, R. *ACS Appl. Mater. Interfaces* **2011**, *3*, 3988−3996.
(8) Liu, J.; Zhao, Y.; Shi, L.; Yuan, S.; Fang, J.; Wang, Z.; Zhang, M. *ACS Appl. Mater. Interfaces* **2011**, *3*, 1261−1268.
(9) Zhang, Y.; Deng, B.; Zhang, T.; Gao, D.; Xu, A.-W. *J. Phys. Chem. C* **2010**, *114*, 5073−5079.
(10) Yang, H. G.; Sun, C. H.; Qiao, S. Z.; Zou, J.; Liu, G.; Smith, S. C.; Cheng, H. M.; Lu, G. Q. *Nature* **2008**, *453*, 638−641.
(11) Wen, C. Z.; Jiang, H. B.; Qiao, S. Z.; Yang, H. G.; Lu, G. Q. *J. Mater. Chem.* **2011**, *21*, 7052−7061.
(12) Liu, S.; Yu, J.; Jaroniec, M. *Chem. Mater.* **2011**, *23*, 4085−4093.
(13) Liu, G.; Yu, J. C.; Lu, G. Q.; Cheng, H.-M. *Chem. Commun.* **2011**, *47*, 6763−6783.
(14) Pan, J.; Liu, G.; Lu, G. Q.; Cheng, H.-M. *Angew. Chem., Int. Ed.* **2011**, *50*, 2133−2137.
(15) Liu, S.; Yu, J.; Jaroniec, M. *J. Am. Chem. Soc.* **2010**, *132*, 11914−11916.
(16) Han, X.; Kuang, Q.; Jin, M.; Xie, Z.; Zheng, L. *J. Am. Chem. Soc.* **2009**, *131*, 3152−3153.
(17) Xiang, Q.; Yu, J.; Jaroniec, M. *Chem. Commun.* **2011**, *47*, 4532−4534.
(18) Wang, Y.; Zhang, H.; Han, Y.; Liu, P.; Yao, X.; Zhao, H. *Chem. Commun.* **2011**, *47*, 2829−2831.
(19) Wu, B.; Guo, C.; Zheng, N.; Xie, Z.; Stucky, G. D. *J. Am. Chem. Soc.* **2008**, *130*, 17563−17567.
(20) Chen, J. S.; Tan, Y. L.; Li, C. M.; Cheah, Y. L.; Luan, D.; Madhavi, S.; Boey, F. Y. C.; Archer, L. A.; Lou, X. W. *J. Am. Chem. Soc.* **2010**, *132*, 6124−6130.
(21) Yang, H. G.; Liu, G.; Qiao, S. Z.; Sun, C. H.; Jin, Y. G.; Smith, S. C.; Zou, J.; Cheng, H. M.; Lu, G. Q. *J. Am. Chem. Soc.* **2009**, *131*, 4078−4083.
(22) Dinh, C.-T.; Nguyen, T.-D.; Kleitz, F.; Do, T.-O. *ACS Nano* **2009**, *3*, 3737−3743.
(23) Wen, C. Z.; Hu, Q. H.; Guo, Y. N.; Gong, X. Q.; Qiao, S. Z.; Yang, H. G. *Chem. Commun.* **2011**, *47*, 6138−6140.
(24) Ma, X. Y.; Chen, Z. G.; Hartono, S. B.; Jiang, H. B.; Zou, J.; Qiao, S. Z.; Yang, H. G. *Chem. Commun.* **2010**, *46*, 6608−6610.
(25) Xiang, Q.; Yu, J.; Wang, W.; Jaroniec, M. *Chem. Commun.* **2011**, *47*, 6906−6908.
(26) Yu, J.; Xiang, Q.; Ran, J.; Mann, S. *CrystEngComm* **2010**, *12*, 872−879.
(27) Yu, J.; Fan, J.; Lv, K. *Nanoscale* **2010**, *2*, 2144−2149.
(28) Lv, K.; Xiang, Q.; Yu, J. *Appl. Catal., B* **2011**, *104*, 275−281.
(29) Lv, K.; Yu, J.; Fan, J.; Jaroniec, M. *CrystEngComm* **2011**, *13*, 7044−7048.
(30) Yu, J.; Dai, G.; Xiang, Q.; Jaroniec, M. *J. Mater. Chem.* **2011**, *21*, 1049−1057.
(31) Liu, B.; Aydil, E. S. *Chem. Commun.* **2011**, *47*, 9507−9509.
(32) Dai, Y.; Cobley, C. M.; Zeng, J.; Sun, Y.; Xia, Y. *Nano Lett.* **2009**, *9*, 2455−2459.
(33) D'Arienzo, M.; Carbajo, J.; Bahamonde, A.; Crippa, M.; Polizzi, S.; Scotti, R.; Wahha, L.; Morazzoni, F. *J. Am. Chem. Soc.* **2011**, *133*, 17652−17661.
(34) Tachikawa, T.; Yamashita, S.; Majima, T. *J. Am. Chem. Soc.* **2011**, *133*, 7197−7204.
(35) Chen, C.; Ma, W.; Zhao, J. *Chem. Soc. Rev.* **2010**, *39*, 4206−4219.
(36) Wang, Q.; Chen, C.; Zhao, D.; Ma, W.; Zhao, J. *Langmuir* **2008**, *24*, 7338−7345.
(37) Pan, L.; Zou, J.-J.; Zhang, X.; Wang, L. *J. Am. Chem. Soc.* **2011**, *133*, 10000−10002.
(38) Yu, J.; Liu, S.; Yu, H. *J. Catal.* **2007**, *249*, 59−66.
(39) Yu, J.; Zhang, J. *Dalton Trans.* **2010**, *39*, 5860−5867.
(40) Fujishima, A.; Zhang, X.; Tryk, D. A. *Surf. Sci. Rep.* **2008**, *63*, 515−582.
(41) Kalyanasundaram, K.; Grätzel, M. *Coord. Chem. Rev.* **1998**, *177*, 347−414.
(42) Xiang, Q.; Lv, K.; Yu, J. *Appl. Catal., B* **2010**, *96*, 557−564.
(43) Yu, J.; Wang, W.; Cheng, B.; Su, B-L. *J. Phys. Chem. C* **2009**, *113*, 6743−6750.

■ NOTE ADDED AFTER ASAP PUBLICATION

This paper was published on the Web on February 23, 2012, with minor text errors in the Experimental Section. The corrected version was reposted on March 14, 2012.